ACADEMIC PRESS

Available online at www.sciencedirect.com
SCIENCE DIRECT®

Journal of Catalysis 218 (2003) 32–41

JOURNAL OF CATALYSIS

www.elsevier.com/locate/jcat

Crystalline $CrV_{1-x}P_xO_4$ catalysts for the vapor-phase oxidation of 3-picoline

Zhaoxia Song, Toshiyuki Matsushita, Tetsuya Shishido, and Katsuomi Takehira *

Department of Chemistry and Chemical Engineering, Graduate School of Engineering, Hiroshima University, 1-4-1 Kagamiyama, Higashi-Hiroshima 739-8527, Japan

Received 28 August 2002; revised 12 February 2003; accepted 19 February 2003

Abstract

The heterogeneously catalyzed vapor-phase oxidation of 3-picoline to nicotinic acid over a series of mixed oxides, $CrV_{1-x}P_xO_4$, was investigated at 300–400 °C. Characterizations of the catalysts were carried out using X-ray diffraction, FT-IR, TG-DTA, BET, NH_3-TPD, TPR, and pyridine adsorption diffuse reflectance infrared Fourier-transform spectra (DRIFTS). The mixed oxides, $CrV_{1-x}P_xO_4$ (x = 0–1.0), were precipitated by adjusting the pH from an aqueous solution of the mixture of the raw materials. The precipitates were calcined at 550–700 °C and employed as the catalyst for the selective oxidation of 3-picoline. During the calcination, a crystallization of monoclinic $CrVO_4$-I phase of α-$MnMoO_4$ structure was clearly observed by TG-DTA, FT-IR, and XRD analyses of the $CrV_{1-x}P_xO_4$, in the range of $x < 0.1$. In these $CrV_{1-x}P_xO_4$, P atoms replace V atoms in the VO_4 tetrahedra still keeping a monoclinic $CrVO_4$-I structure. This structure changed to amorphous by further addition of P ($x > 0.25$) or to orthorhombic $CrVO_4$-III by further calcination at high temperature (> 700 °C), resulting in the catalyst deactivation. It was found that $CrVO_4$-I was originally active and the addition of a small amount of P resulted in a high enhancement in the catalytic activity; $CrV_{0.95}P_{0.05}O_4$ showed the highest activity among the catalysts tested. NH_3-TPD showed an increase in the acid site by replacing V with a small amount of P in $CrVO_4$-I. A favorable effect of water addition suggests that Brönsted acid assists the selective oxidation, and this was confirmed by infrared study of pyridine adsorption on the catalysts. The active catalysts, $CrV_{1-x}P_xO_4$ ($0 < x < 0.1$), alone revealed a weak reduction peak of V around 350 °C in the TPR, and the peak temperature was the lowest over the most active catalyst. The reduction–oxidation property was reversibly observed with the peak when the catalyst was treated by H_2 and O_2 atmosphere alternately. Moreover, activation energy calculated from 3-picoline consumption was also the lowest over the most active catalyst. All the V species are isolated as VO_4 tetrahedra in the $CrVO_4$-I structure and considered to work as the active sites via its reduction–oxidation assisted by both chromium and phosphorous atoms. It is concluded that 3-picoline is selectively oxidized on the V sites by the reduction–oxidation further assisted by the Brönsted-acid sites over the crystallized $CrV_{0.95}P_{0.05}O_4$ catalyst.

Keywords: $CrV_{1-x}P_xO_4$ catalysts; Heterogeneous vapor-phase oxidation; Monoclinic $CrVO_4$-I structure; 3-Picoline; Nicotinic acid; V reduction–oxidation sites; Brönsted acid sites

1. Introduction

Solid, heterogeneous catalysts have the advantages of ease of recovery and recycling and are readily amenable to continuous processing. Therefore, the vapor-phase oxidation of organic compounds over the heterogeneous catalysts is environmentally benign from the viewpoint of "green chemistry." The literature on the vapor-phase oxidation of organic compounds catalyzed by binary vanadium oxide catalysts is quite numerous [1,2]. The partial oxidation of 3-picoline has received much attention because its oxidation product, nicotinic acid, is a valuable intermediate for pharmaceuticals and food additives. The vapor-phase oxidation of picolines has been performed on a series of vanadium oxide catalysts, such as V_2O_5 [3], V_2O_5/SnO_2 [4,5], and V_2O_5/TiO_2 [6–9], and $(VO)_2P_2O_7$ [10]. The other vanadium-containing catalysts have also been proposed for the vapor-phase oxidation of substituted methyl aromatics [11–13] and reviewed recently [1,2].

We have reported that a new series of metal vanadates ($Cr_{1-x}Al_xVO_4$) were effective as the catalysts for the vapor-phase oxidation of 3-picoline to nicotinic acid [14,15]. Monoclinic $CrVO_4$-I, which belongs to an α-$MnMoO_4$ structure,

* Corresponding author.
E-mail address: takehira@hiroshima-u.ac.jp (K. Takehira).

0021-9517/03/$ – see front matter
doi:10.1016/S0021-9517(03)00076-9

showed a high activity as well as a high selectivity to nicotinic acid. The activity of $CrVO_4$-I was enhanced when a part of Cr atoms were replaced with Al atoms. The isolated VO_4 tetrahedra in $CrVO_4$-I was considered as the active site via its reduction–oxidation property assisted by Cr atoms in the Cr_4O_{16} clusters, which linked to the other clusters by VO_4 tetrahedra [14,15]. Moreover, it was considered that, by the incorporation of Al in the structure, Al atoms replaced Cr atoms in the Cr_4O_{16} clusters and affected the activity of the VO_4 tetrahedra.

It was reported by Attfield [16] that a replacement of V in $CrVO_4$-I with P is also possible, resulting in the formation of $CrV_{1-x}P_xO_4$ and this compound also belongs to an α-$MnMoO_4$ structure. Indeed, it will be possible to modify the active V–O–Cr sites by replacing V^{5+} with P^{5+} in the VO_4 tetrahedra, considering their ionic radii of 0.40 and 0.35 Å, respectively [17]. Actually we have confirmed and briefly reported the high activity of $CrV_{1-x}P_xO_4$ catalyst for the selective oxidation of 3-picoline [18]. In this paper, we report the details of the structure and the catalytic activities of $CrV_{1-x}P_xO_4$ in the vapor-phase oxidation of 3-picoline.

2. Experimental

2.1. Catalyst preparation

The $CrV_{1-x}P_xO_4$ catalysts were prepared following the method proposed by Touboul and co-workers [19,20]. Aqueous solutions of NH_4VO_3, $Cr(NO_3)_3 \cdot 9H_2O$, and $NH_4H_2PO_4$ were mixed, and the pH value of the solution was lowered to 0.1–1.0 to form transparent and dark green solution by adding 3 N nitric acid aqueous solution. Then, the pH value was raised and adjusted to 4.0 at 50 °C by adding 3 N ammonia aqueous solution, and stirred for 4 h, resulting in the formation of yellowish green precipitate. The precipitate was washed with deionized water, dried at 100 °C overnight, and finally calcined at 550–570 °C in air for 6 h. $CrVO_4$-III as a reference for the catalyst characterization was prepared by calcining a mixture of V_2O_5 and Cr_2O_3 at 800 °C for 10 h.

2.2. Characterization of catalysts

The X-ray diffraction (XRD) was carried out on a Mac Science MX 18XHF-SRA using Cu-K_α-radiation with a scanning range (2θ) from 10 to 70°. Fourier transfer infrared spectroscopy (FT-IR) was recorded on a Shimadzu FTIR-8300 using a KBr disk method. Differential thermal analyses (DTA) were carried out using a Shimadzu DTG-50/50H at a heating rate of 10 °C min^{-1} from room temperature to 1000 °C with α-Al_2O_3 as a reference. BET specific surface areas of the catalysts were measured by N_2 adsorption using a Shimadzu Micromeritics Flow Sorb II 2300 in liquid nitrogen at −196 °C.

The temperature-programmed desorption of ammonia (NH_3-TPD) was performed to scrutinize the acidic properties of the catalysts. Prior to the adsorption of ammonia, the catalyst sample (ca. 150 mg) was pretreated for 1 h in a helium stream at 500 °C. After cooling to 100 °C, the sample was evacuated for 0.5 h and then exposed to 20 Torr of NH_3 for 0.5 h. After adsorption, the gas stream was switched to helium (10 ml min^{-1}) to remove physically adsorbed ammonia from the catalyst surface. The ammonia-desorption profile was measured by a BEL Japan TPD-1-AT at a heating rate of 10 °C min^{-1} from room temperature to 500 °C under 10 ml min^{-1} helium flow. Depending on the catalyst, a small amount of N_2 was detected in the effluent gas probably due to the reduction of the catalyst by NH_3. Temperature-programmed reduction (TPR) of the catalyst was performed with 50 mg of the catalyst at a heating rate of 10 °C min^{-1} using a mixture of 5 vol% H_2/Ar (100 ml min^{-1}) as reducing gas. A TCD was used for monitoring the H_2 consumption after passing through a 13X molecular sieve trap to remove water. Prior to the TPR measurements, the sample was treated at 300 °C for 1 h in 20 vol% O_2/Ar gas (50 ml min^{-1}). To the test reduction–oxidation property of the active site on the catalysts, the catalyst sample was first treated by the TPR from room temperature to 350 °C and followed by the TPR again to 350 °C without any treatment after cooling. Finally the catalyst was treated by the TPR after the reoxidizing treatment with a mixture of 20 vol% O_2/Ar (50 ml min^{-1}) at 350 °C for 1 h and an appearance of the reduction peak of reoxidized active sites was confirmed.

The diffuse reflectance infrared Fourier-transform spectra (DRIFTS) were recorded with a Nicolet MAGNA-IR 560 spectrometer equipped with an in situ collector diffuse reflectance cell. Spectra were obtained from a narrow band MCT detector by 128 scans at 4 cm^{-1} resolution. The sample powder (ca. 40 mg) in an in situ diffuse reflectance cell with NaCl windows was pretreated at 500 °C in N_2 flow. The flow rate of each gas was controlled by a STEC Model SEC400-MK3 mass flow controller, and gases were delivered to the sample at atmospheric pressure. The pretreated sample was exposed to 3.2% pyridine in N_2 flow at 30 ml min^{-1} for 10 min at 30 °C. The sample was then purged at 30 °C for 30 min in N_2 flow at 30 ml min^{-1} to remove gas-phase species, after which the temperature was increased to 180 °C, while continuing to flow N_2 at 30 ml min^{-1} to remove the physisorbed pyridine. After cooling to 30 °C, the sample was exposed to 2.3% H_2O in N_2 flow at 30 ml min^{-1} for 10 min and then purged at 30 °C for 30 min in N_2 flow at 30 ml min^{-1}.

2.3. Catalytic testing

The catalytic tests were conducted in a fixed-bed reactor at atmospheric pressure and at temperatures from 300 to 400 °C. A Pyrex glass tube reactor with 20-cm length by 8-mm i.d. was used in an electrically heated oven. The 0.2 g catalyst powder was made to pellet and crushed into

particles with the sizes of 26–42 mesh; these were filled at the bottom of the tube diluted with quartz sand. The catalyst was activated in an oxygen/nitrogen mixed gas flow (18/33 ml min^{-1}) at 540 °C for 1 h and then settled down to the reaction temperature under the O_2/N_2 mixed gas flow. The liquid mixture of 3-picoline and water was passed through a vaporization zone at 200 °C, mixed with oxygen and nitrogen as the carrier gas, and finally fed in to the reactor. The line from the vaporizer to the reactor was heated to a temperature above 250 °C. The feed composition of 3-picoline/H_2O was varied from 1/0 to 1/108 (molar ratio) under a constant gas hourly space velocity around 38,000 ml $h^{-1} g_{cat}^{-1}$. Water, 3-picoline, pyridine-3-carbaldehyde, and nicotinic acid were condensed after the reactor, and all samples were analyzed by a FID gas chromatograph. The inorganic components (CO, CO_2, O_2, and N_2) were analyzed by an on-line TCD gas chromatograph. HCN was not determined, even though its formation has been frequently reported in the literature [1,6].

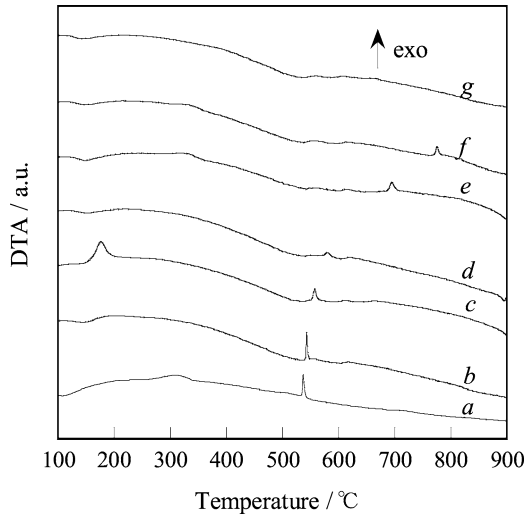

Fig. 1. DTA curves of the $CrV_{1-x}P_xO_4$ catalysts. (a) $CrVO_4$, (b) $CrV_{0.98}P_{0.02}O_4$, (c) $CrV_{0.95}P_{0.05}O_4$, (d) $CrV_{0.9}P_{0.1}O_4$, (e) $CrV_{0.75}P_{0.25}O_4$, (f) $CrV_{0.5}P_{0.5}O_4$, and (g) $CrPO_4$.

3. Results and discussion

3.1. Structure of $CrV_{1-x}P_xO_4$ catalysts

The $CrV_{1-x}P_xO_4$ catalysts used in the present work are shown in Table 1, together with the calcination temperature and the surface area. The number in parentheses in each catalyst symbol shows the temperature of calcination. The calcination temperature was selected based on the results obtained by DTA measurement. DTA curves of the precursors of $CrV_{1-x}P_xO_4$ after the drying are shown in Fig. 1. Several broad endo- and exothermic peaks observed below 400 °C along with substantial weight decreases in TGA may be due to the loss of water and the decomposition of ammonium nitrate formed in the precursors. A sharp exothermic peak appeared at 538 °C with $CrVO_4$ (Fig. 1, a) and was assigned to the crystallization of $CrVO_4$-I by Touboul and Melghit [20]. The temperature of this exothermic peak increased gradually with increasing x in $CrV_{1-x}P_xO_4$ (Fig. 1, b, c, d, e, and f) and finally disappeared with $CrPO_4$ (Fig. 1, g) in the temperature range below 900 °C. This crystallization to $CrVO_4$-I phase was clearly confirmed in the results of XRD measurements as shown in the following paragraph.

Fig. 2 shows the XRD patterns of $CrV_{1-x}P_xO_4$ ($x = 0$, 0.02, 0.05, 0.1, 0.25, 0.5, and 1). The diffraction lines of monoclinic $CrVO_4$-I (α-$MnMoO_4$ structure) [20–23] were distinctly observed for $CrV_{1-x}P_xO_4$ ($0 \leqslant x \leqslant 0.25$) (Fig. 2, a, b, d, e, g, and h). The crystallization to the $CrVO_4$-I structure during calcination was clearly observed

Table 1
Calcination temperature and BET surface area of the $CrV_{1-x}P_xO_4$ catalysts

Catalysts	Calcination temperature (°C)	Surface area ($m^2 g^{-1}$)
$CrVO_4$(550)	550	24.5
$CrV_{0.98}P_{0.02}O_4$(570)	570	22.4
$CrV_{0.95}P_{0.05}O_4$(350)	350	103.6
$CrV_{0.95}P_{0.05}O_4$(570)	570	21.1
$CrV_{0.90}P_{0.10}O_4$(570)	570	19.1
$CrV_{0.75}P_{0.25}O_4$(570)	570	52.9
$CrV_{0.75}P_{0.25}O_4$(650)	650	16.5
$CrV_{0.75}P_{0.25}O_4$(700)	700	17.9
$CrV_{0.50}P_{050}O_4$(700)	700	14.8
$CrPO_4$(700)	700	6.4

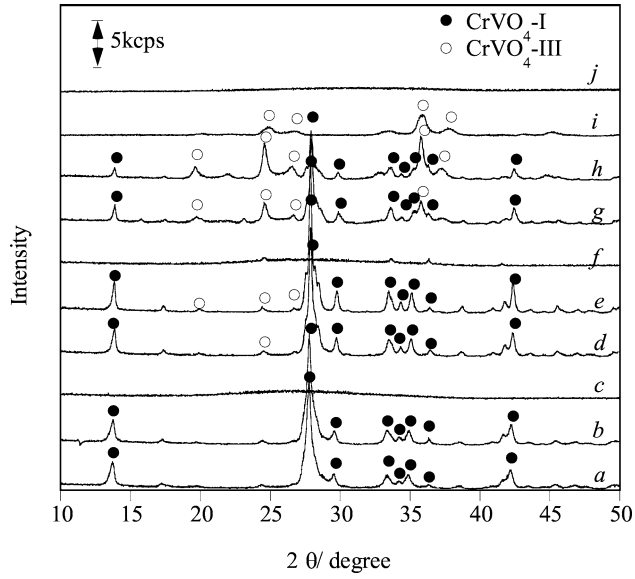

Fig. 2. XRD patterns of the $CrV_{1-x}P_xO_4$ catalysts. (a) $CrVO_4$ (550), (b) $CrV_{0.98}P_{0.02}O_4$(570), (c) $CrV_{0.95}P_{0.05}O_4$(350), (d) $CrV_{0.95}P_{0.05}O_4$(570), (e) $CrV_{0.9}P_{0.1}O_4$(570), (f) $CrV_{0.75}P_{0.25}O_4$(570), (g) $CrV_{0.75}P_{0.25}O_4$(650), (h) $CrV_{0.75}P_{0.25}O_4$(700), (i) $CrV_{0.5}P_{0.5}O_4$ (700), and (j) $CrPO_4$(700).

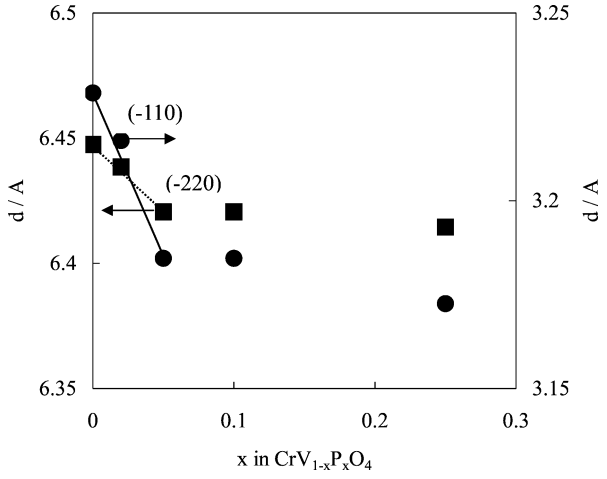

Fig. 3. Vegard's plots of (−110) and (−220) planes of the $CrV_{1-x}P_xO_4$ catalysts.

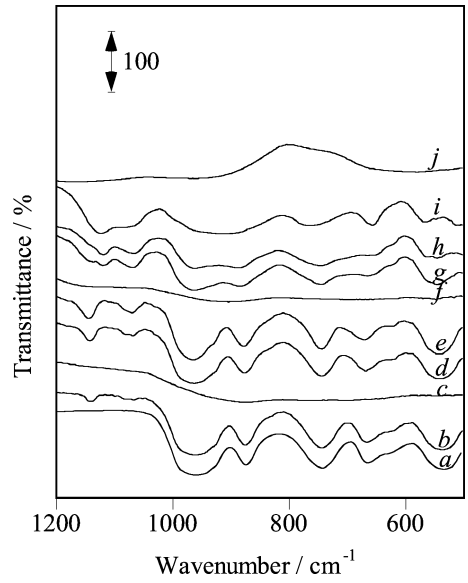

Fig. 4. FT-IR spectra of the $CrV_{1-x}P_xO_4$ catalysts. (a) $CrVO_4$ (550), (b) $CrV_{0.98}P_{0.02}O_4$(570), (c) $CrV_{0.95}P_{0.05}O_4$(350), (d) $CrV_{0.95}P_{0.05}O_4$(570), (e) $CrV_{0.9}P_{0.1}O_4$(570), (f) $CrV_{0.75}P_{0.25}O_4$(570), (g) $CrV_{0.75}P_{0.25}O_4$(650), (h) $CrV_{0.75}P_{0.25}O_4$(700), (i) $CrV_{0.5}P_{0.5}O_4$ (700), and (j) $CrPO_4$(700).

with all catalysts, among those two typical examples, i.e., $CrV_{0.95}P_{0.05}O_4$ and $CrV_{0.75}P_{0.25}O_4$, are shown in Fig. 2. The $CrV_{0.95}P_{0.05}O_4$ sample was amorphous after the calcination at 350 °C (c) and well crystallized to monoclinic $CrVO_4$-I structure after the calcination at 570 °C (d). In the case of $CrV_{0.75}P_{0.25}O_4$, the amorphous phase was still observed even after the calcination at 570 °C (f), while the crystallized phases of both $CrVO_4$-I and $CrVO_4$-III were detected after the calcination at 650 °C (g), and the crystallinity increased with increasing the calcination temperature to 700 °C (h). In both samples of $CrV_{0.95}P_{0.05}O_4$ and $CrV_{0.75}P_{0.25}O_4$, it was shown that the crystallization of $CrVO_4$-I took place around the exothermic peak temperature in the DTA curves (Fig. 1).

The diffraction lines of monoclinic $CrVO_4$-I phase were observed exclusively with the $CrV_{1-x}P_xO_4$ catalysts of $0 \leqslant x \leqslant 0.05$ and, moreover, the diffraction lines of both (−110) and (−220) planes shifted toward the lower d values with increasing x following Vegard's law as shown in Fig. 3. These results strongly suggest that P atoms were incorporated in the structure of $CrVO_4$-I probably by replacing the sites of V in the VO_4 tetrahedra linking the Cr_4O_{16} clusters, taking into account the smaller ionic radius of P^{5+} (0.35 Å) than V^{5+} (0.40 Å) [17]. When x increased to 0.5 in $CrV_{1-x}P_xO_4$, the $CrVO_4$-III phase alone was observed (Fig. 2, i), even though the diffraction lines were weak and broad. A totally replaced $CrPO_4$ showed only an amorphous phase even after the calcination at 700 °C (j). Different hydrates of $CrPO_4$ are known [23]; their calcinations at high temperature allow the anhydrous material to be formed in two types of their polymorphic forms: β-$CrPO_4$ above 1000 °C and α-$CrPO_4$ above 1175 °C. Thus, amorphous $CrPO_4$ is stable and does not crystallize even at high temperature of 900 °C in the DTA curves (Fig. 1).

$CrVO_4$-I crystallizes in a monoclinic system, $a = 9.791$ (6) Å, $b = 8.848(5)$ Å, $c = 6.843(6)$ Å, and $\beta = 107.8(1)$ Å; $Dx = 3.98$ with $Z = 8$; and space group $C2/m$ [21]. Numbers I and III refer to the parent $InVO_4$ forms [24,25]. The orthorhombic form of $CrVO_4$, $CrVO_4$-III, is isostructural to the $InVO_4$-III [20,22,25]. It is reported that orthorhombic $CrVO_4$ ($CrVO_4$-III) was obtained by heating $CrVO_4$-I at 660 °C [20]. Those of $CrVO_4$-III appeared clearly for both $CrV_{0.75}P_{0.25}O_4$ and $CrV_{0.5}P_{0.5}O_4$ (Fig. 2, g, h, and i), when the catalysts were calcined at temperatures above 650 °C. $CrVO_4$(550) (a), $CrV_{0.98}P_{0.02}O_4$(570) (b), $CrV_{0.95}P_{0.05}O_4$(570) (d), and $CrV_{0.9}P_{0.1}O_4$(570) (e) mainly showed the pattern of $CrVO_4$-I, while both $CrV_{0.75}P_{0.25}O_4$ (650) (g) and $CrV_{0.75}P_{0.25}O_4$(700) (h) showed both patterns of $CrVO_4$-I and $CrVO_4$-III.

FT-IR spectra of $CrV_{1-x}P_xO_4$ (Fig. 4) well correlated with the results of XRD analyses. The $CrV_{1-x}P_xO_4$ catalysts containing P in the range of $0 \leqslant x \leqslant 0.02$ (Fig. 4, a and b) showed the adsorption bands at 960, 925, 875, 744, and 667 cm^{-1}, probably assigned to V–O–V, V–O–Cr and Cr–O–Cr stretching vibrations of the monoclinic $CrVO_4$-I structure. An increase in the P contents ($0.02 \leqslant x \leqslant 0.10$) resulted in a blue shift of the bands of $CrVO_4$-I, indicating that some V–O–V bonds are replaced by V–O–P. Moreover, new absorption bands appeared between 1000 and 1200 cm^{-1} probably assigned to some P–O vibrations as observed in the α-$CrPO_4$ phase [23] (Fig. 4, d and e). When the P contents increased to $0.25 \leqslant x \leqslant 0.5$ (Fig. 4, g, h, and i), the spectra changed substantially and became close to that of α-$CrPO_4$ [23]. $CrV_{0.98}P_{0.02}O_4$(350) (Fig. 4, c), $CrV_{0.75}P_{0.25}O_4$(570) (Fig. 4, f), and $CrPO_4$(700) (Fig. 4, j) showed no absorption bands probably due to their amorphous structures, because of calcination temperatures too low to crystallize.

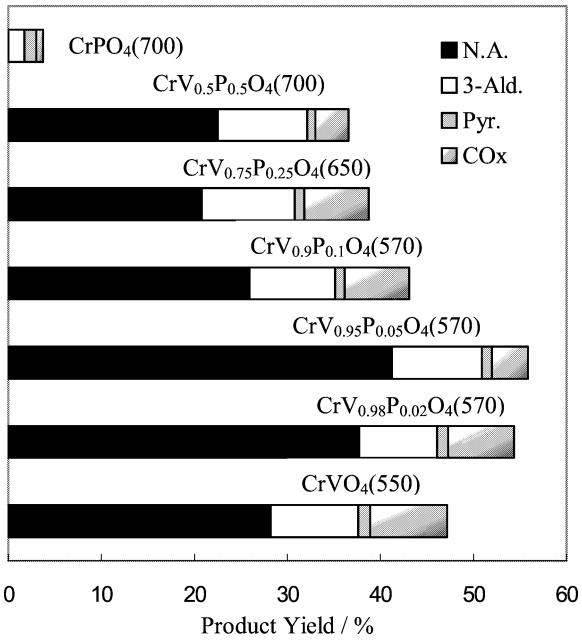

Fig. 5. Oxidation of 3-picoline over the $CrV_{1-x}P_xO_4$ catalysts. 3-Picoline/$H_2O/O_2/N_2 = 0.75/8.1/18/100$ ml_{NTP} min^{-1}. Reaction temperature 350 °C.

3.2. Oxidation of 3-picoline

Oxidation of 3-picoline was performed over $CrV_{1-x}P_xO_4$ catalysts from 300 to 400 °C under the feed composition of 3-picoline/$H_2O/O_2/N_2$ of 0.75/8.1/18/100 ml_{NTP} min^{-1} (molar ratio of 1/10.8/24/134). The main products were nicotinic acid and pyridine-3-carbaldehyde, and CO_2 was observed as a by-product together with a trace amount of pyridine. Mass balance calculated between 3-picoline conversion and yields of the products was above 95% in all reactions. Fig. 5 shows the yields of nicotinic acid (N.A.), pyridine-3-carbaldehyde (3-Ald.), carbon oxide (CO_x) and pyridine (Pyr.), in the oxidation of 3-picoline over 0.2 g of $CrV_{1-x}P_xO_4$ ($x = 0$–1.0) at 350 °C. A small amount of pyridine was observed over all the catalysts including $CrPO_4$(700) and probably formed by decarboxylation of nicotinic acid. $CrV_{0.95}P_{0.05}O_4$(570) showed the highest yields of nicotinic acid and pyridine-3-carbaldehyde, followed by $CrV_{0.98}P_{0.02}O_4$(570), although their surface areas were lower than $CrVO_4$(550). When x exceeded 0.05, the yields gradually decreased with increasing x, and finally $CrPO_4$(700) showed a sudden decline in the activity, resulting in no formation of nicotinic acid. It is thus suggested that the $CrVO_4$-I structure is important for the selective oxidation of 3-picoline and a small amount of phosphorus assists the catalytic activity of $CrVO_4$-I.

This suggestion was confirmed by the further studies on the effect of the calcination temperature of $CrV_{0.95}P_{0.05}O_4$ and $CrV_{0.75}P_{0.25}O_4$. Yields of the products per surface area of the catalysts are shown in Fig. 6 for both $CrV_{0.95}P_{0.05}O_4$ and $CrV_{0.75}P_{0.25}O_4$ calcined at different temperatures. When $CrV_{0.95}P_{0.05}O_4$ was calcined at 350 °C, the activity

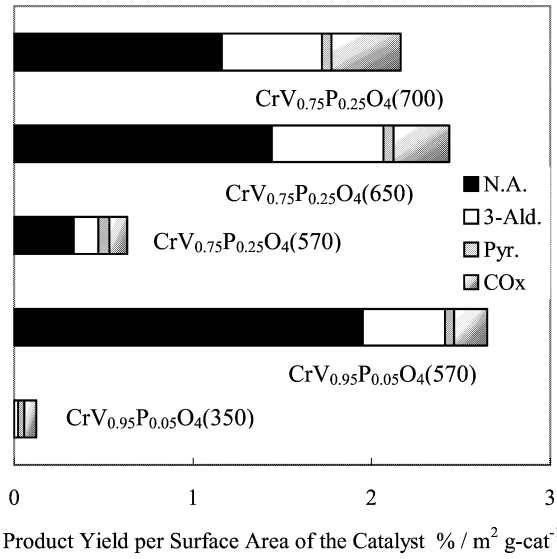

Fig. 6. Oxidation of 3-picoline over the $CrV_{1-x}P_xO_4$ catalysts—Effect of the calcination temperature. 3-Picoline/$H_2O/O_2/N_2 = 0.75/8.1/18/100$ ml_{NTP} min^{-1}. Reaction temperature 350 °C.

was extremely low. By the calcination at 570 °C, the activity increased to the highest value among the catalysts tested. Also in the case of $CrV_{0.75}P_{0.25}O_4$, the calcination temperature showed a distinct effect on the activity. The calcination at 570 °C afforded a low activity, while those at 650 and 700 °C caused a substantial increase in the activity. These critical features can be explained by the change in the catalyst structure from amorphous to crystalline. As observed in the analytical results of the catalysts by XRD (Fig. 2) and IR (Fig. 4), the amorphous phases of $CrV_{0.95}P_{0.05}O_4$(350) (Fig. 2, c, and Fig. 4, c) and $CrV_{0.75}P_{0.25}O_4$(570) (Fig. 2, f and Fig. 4, f) changed to the crystalline phases of $CrV_{0.95}P_{0.05}O_4$(570) (Fig. 2, d, and Fig. 4, d), $CrV_{0.75}P_{0.25}O_4$(650) (Fig. 2, g, and Fig. 4, g) and $CrV_{0.75}P_{0.25}O_4$(700) (Fig. 2, h, and Fig. 4, h) by increasing the calcination temperature. The critical temperatures of these phase transitions from amorphous to crystalline are supported by the results of DTA (Fig. 1, b and e), showing the exothermic peak at 543 and 695 °C due to the crystallization of the monoclinic $CrVO_4$-I structure. The temperature of 650 °C does not seems high enough, but may be recovered by calcination for 6 h for assisting the crystallization of the $CrVO_4$-I structure in $CrV_{0.75}P_{0.25}O_4$(650). It will be concluded that the monoclinic $CrVO_4$-I-based structure is important in the selective oxidation of 3-picoline and the activity is enhanced by the incorporation of phosphorus in the V-site in the structure.

3.3. Optimization of the reaction conditions

It is frequently reported that the addition of water enhances the yield of nicotinic acid in the vapor-phase oxidation of 3-picoline [1,2,4–7]. We have also confirmed the favorable effect of water in the oxidation of 3-picoline over

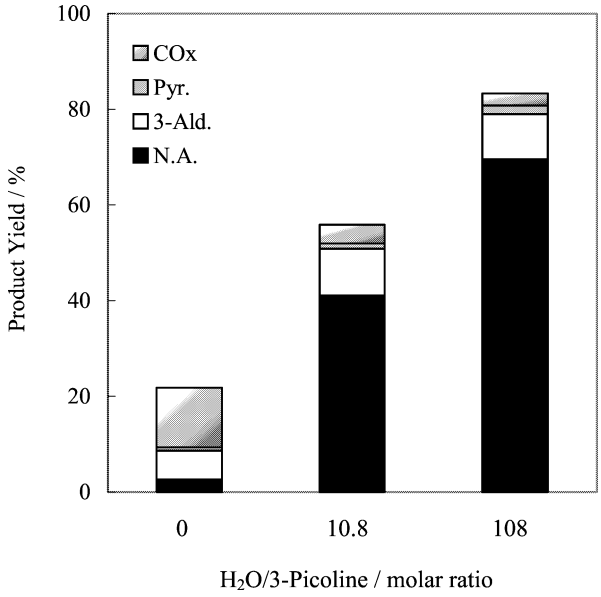

Fig. 7. Effect of water addition on the yields of products in the oxidation of 3-picoline over $CrV_{0.95}P_{0.05}O_4$(570). Reaction temperature 350 °C.

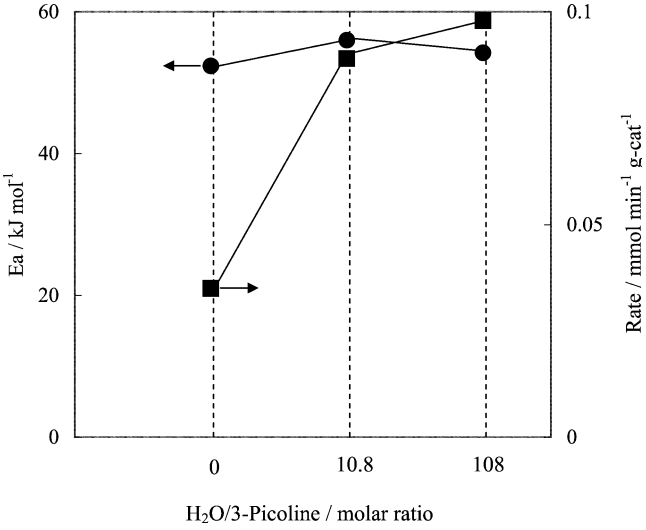

Fig. 8. Effect of water addition on the oxidation of 3-picoline over $CrV_{0.95}P_{0.05}O_4$(570). Reaction temperature 350 °C.

$Cr_{0.5}Al_{0.5}VO_4$, which afforded nicotinic acid (yield, 58.9%) and pyridine-3-carbaldehyde (yield, 10.0%) in the presence of water at the ratio of H_2O/3-picoline = 108/1(15). The results of 3-picoline oxidation over $CrV_{0.95}P_{0.05}O_4$(570) at 350 °C in the presence of water are shown in Figs. 7 and 8. Both yield and selectivity of nicotinic acid were very low in the absence of water, while the addition of water enhanced enormously the selective oxidation of 3-picoline to nicotinic acid (Fig. 7). Major products were carbon oxide and pyridine from 3-picoline in the absence of water, and in turn substantially changed to nicotinic acid and pyridine-3-carbaldehyde in the presence of water. The rate of 3-picoline consumption was also enhanced by the addition of water; however, apparent activation energy calculated from the rate of 3-picoline

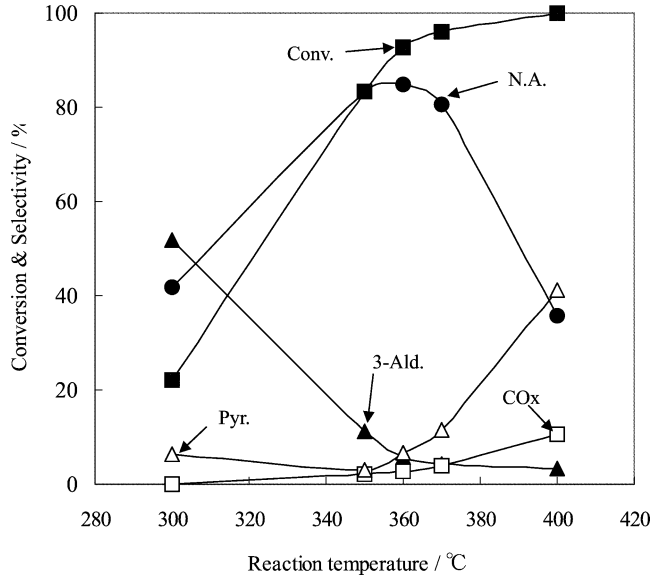

Fig. 9. Effect of the reaction temperature on the oxidation of 3-picoline over $CrV_{0.95}P_{0.05}O_4$. 3-Picoline/H_2O/O_2/N_2 = 0.52/56.9/16.3/30.0 ml_{NTP} min^{-1}.

consumption was almost constant independent of the amount of water (Fig. 8). This indicates that the rate-determining step does not relate directly to the acid sites enhanced by water addition.

The effect of reaction temperature in the 3-picoline oxidation over $CrV_{0.95}P_{0.05}O_4$(570) in the presence of an excess amount of water (H_2O/3-picoline = 108) is shown in Fig. 9. Increasing temperature is profitable for the selective oxidation of 3-picoline to nicotinic acid and the optimum temperature was found to be 360 °C, giving the highest yields of nicotinic acid (78.4%) and pyridine-3-carbaldehyde (5.4%) at the conversion of 92.6%. However, when the reaction temperature was further increased, the temperature became hard to be controlled, resulting in a drastic decrease in the selectivity to nicotinic acid. The activity of $CrV_{0.95}P_{0.05}O_4$(570) for nicotinic acid production was far higher than that of $Cr_{0.5}Al_{0.5}VO_4$ previously reported [14,15], i.e., the yields of nicotinic acid (58.9%) and pyridine-3-carbaldehyde (10.0%) at the conversion of 80.4%. It was reported that V_2O_5/TiO_2 catalyzed the selective oxidation of 3-picoline at 250–280 °C and afforded nicotinic acid with the selectivity above 90% at the conversion above 90% [6,7]. However only anatase TiO_2 was effective as the support and is possibly transformed to rutile TiO_2, resulting in deactivation, during the exothermic reaction. On the other hand, $CrV_{0.95}P_{0.05}O_4$(570) is thermally stable and a promising catalyst for the oxidation reaction.

3.4. Acid sites on the catalysts

The results of NH_3-TPD (Fig. 10) showed an increase in the amount of acid sites by the addition of P up to $x = 0.05$ and the decrease with the further increase in the P content. $CrVO_4$-III as a reference was also tested and compared

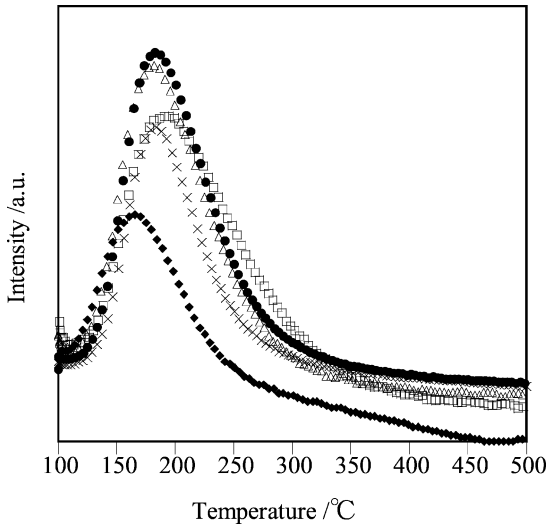

Fig. 10. NH_3-TPD of the $CrV_{1-x}P_xO_4$ catalysts. (×) $CrVO_4$(550), 150 mg; (●) $CrV_{0.95}P_{0.05}O_4$(570), 150 mg; (△) $CrV_{0.75}P_{0.25}O_4$(650), 150 mg; (□) $CrV_{0.5}P_{0.5}O_4$(700), 150 mg; (◆) $CrVO_4$-III, 6030 mg.

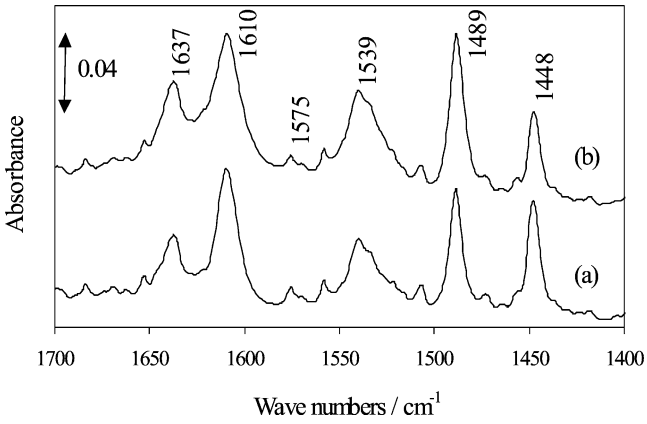

Fig. 11. DRIFTS of pyridine adsorbed on $CrV_{0.95}P_{0.05}O_4$(570). (a) Before and (b) after introduction of H_2O.

with the other catalysts of a $CrVO_4$-I-type crystal structure. A large amount of $CrVO_4$-III was used considering that the surface area was very small (0.61 $m^2\,g_{cat}^{-1}$). The amount of acid sites estimated from the NH_3-TPD results varied considerably depending on the P content. However, the temperature at the peak top of NH_3-TPD was almost constant with all the catalysts tested including $CrVO_4$-III, suggesting that the strength of the acid site was not substantially affected by the addition of P. Thus, the acid nature of the catalyst alone cannot explain the kinetics of the oxidation of 3-picoline to nicotinic acid. In the NH_3-TPD, a weak and broad peak of N_2 was observed around 235 °C over $CrV_{0.95}P_{0.05}O_4$ catalysts, but the other catalysts showed no peak of N_2 at any temperature. The temperature of N_2 evolution was somewhat higher than that of NH_3 desorption around 190 °C, suggesting that the catalyst was reduced by NH_3. It is likely that the addition of P enhanced the reducibility of V in the catalyst.

The results of the pyridine adsorbed DRIFTS measurements are shown in Fig. 11. When pyridine was adsorbed on the pretreated $CrV_{0.95}P_{0.05}O_4$(570) (a), several absorption bands were observed and can be assigned based on the results reported with vanadyl pyrophosphate [26] and VPO/TiO_2 [27] catalysts, as follows. The bands at 1610, 1575, 1489, and 1448 cm^{-1} are assigned to vibrations of pyridine molecules adsorbed through coordinative interaction with Lewis acid surface sites (L-Py), while the bands at 1637, 1610, 1539, and 1489 cm^{-1} are assigned to vibrations of pyridine molecules adsorbed on Brönsted acid sites (B-Py). Among these bands, the band at 1489 cm^{-1} contains contributions due to vibration of both pyridinium ions (B-Py) and coordinatively adsorbed pyridine molecules (L-Py). The band at 1610 cm^{-1} is also probably due to vibration to both 8b of pyridinium ions (B-Py) and 8a of coordinated pyridines (L-Py). These results indicate that both Brönsted and Lewis acid sites are present on the pretreated $CrV_{0.95}P_{0.05}O_4$(570) surface. Upon exposure of the $CrV_{0.95}P_{0.05}O_4$(570) sample to water vapor (Fig. 11, b), the intensity of the band at 1448 cm^{-1} (L-Py) decreased significantly, while that of the band at 1539 cm^{-1} (B-Py) increased. The ratio of intensities of the bands at 1539 and 1448 cm^{-1} (B-Py/L-Py) changed from 0.96 to 2.27 by exposure to water vapor. This result indicates that a part of Lewis acid sites on the surface of $CrV_{0.95}P_{0.05}O_4$(570) was converted to Brönsted acid sites by the addition of water vapor [28]. Water should also contribute in the hydrolysis of V–O–P bonds resulting in the formation of new Brönsted acid sites. The remarkable increase in the activity in the presence of water (Fig. 8) can be well explained by this increase in Brönsted acid sites, i.e., Brönsted acid sites contributes rather strongly to the catalytic activity of $CrV_{1-x}P_xO_4$ than Lewis acid sites as already reported [6]. It must be also noted that the effect of water is not only in the enhancement of Brönsted acid sites but also in preventing the nonreactive irreversible absorption of 3-picoline as well as in the desorption of nicotinic acid [29]. The higher acidity may enhance the selectivity to nicotinic acid, probably due to a quick desorption of the acid, which will be protected from further deep oxidation.

3.5. Reduction–oxidation sites on the catalysts

TPR results are shown in Fig. 12. A main peak of H_2 consumption was observed at increasing temperatures with increasing P contents, i.e., 521, 527, 541, 561, 598, and 623 °C for $CrVO_4$(550) (a), $CrV_{0.98}P_{0.02}O_4$(570) (b), $CrV_{0.95}P_{0.05}O_4$(570) (c), $CrV_{0.90}P_{0.10}O_4$(570) (d), $CrV_{0.75}P_{0.25}O_4$(650) (e), and $CrV_{0.50}P_{0.50}O_4$(700) (f), respectively. The amount of H_2 consumed decreased with increasing P content, suggesting that V species in the catalyst are reduced. $CrPO_4$(700) (g) revealed a clearly different curve from the others. $CrVO_4$-III (h) as the reference showed two peaks at 638 and 730 °C, showing that the V species in $CrVO_4$-III is more stable than that in $CrVO_4$-I against the reduction. Interestingly, additional peaks were observed at temperatures lower than the main peak only in the TPR of the active catalysts, i.e., $CrVO_4$(550) (a), $CrV_{0.98}P_{0.02}O_4$(570)

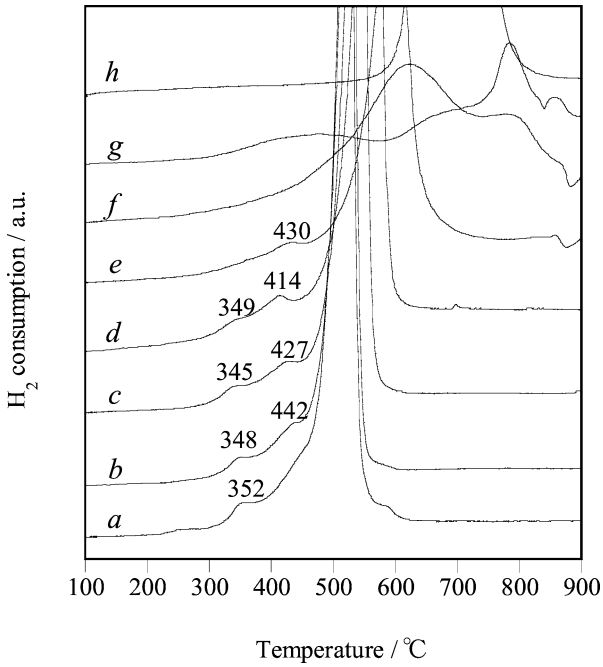

Fig. 12. TPR profiles of the catalysts. (a) $CrVO_4$(550), (b) $CrV_{0.98}P_{0.02}O_4$(570), (c) $CrV_{0.95}P_{0.05}O_4$(570), (d) $CrV_{0.9}P_{0.1}O_4$ (570), (e) $CrV_{0.75}P_{0.25}O_4$(650), (f) $CrV_{0.50}P_{0.50}O_4$(700), (g) $CrPO_4$ (700), and (h) $CrVO_4$-III.

(b), $CrV_{0.95}P_{0.05}O_4$(570) (c), $CrV_{0.90}P_{0.10}O_4$(570) (d), and $CrV_{0.75}P_{0.25}O_4$(650) (e); the first peak appeared around 350 °C and the second one around 430 °C. The temperature of the first peak almost coincided with the temperature that afforded the highest yield of nicotinic acid in Fig. 9, suggesting that catalyst reduction around 350 °C is important in the catalytic activity. This temperature varied depending on the P content, and the lowest value, 345 °C, was observed with the catalyst giving the highest activity, i.e., $CrV_{0.95}P_{0.05}O_4$(570) (c). The lowest value of the reduction temperature may well relate to the easy reduction of $CrV_{0.95}P_{0.05}O_4$(570) proved by the formation of N_2 during the NH_3-TPD. Moreover, the reduction at the first peak was reversibly observed after the reoxidation. After the TPR from room temperature to 350 °C, the catalyst was again treated by the TPR, where no reduction peak was observed any more since all active V species have been reduced during the first TPR. However, when the catalyst was treated by O_2 gas at 350 °C for 1 h, the reduction peak appeared again around 350 °C in the TPR. This shows clearly that the reversible reduction–oxidation took place on the V sites around 350 °C and contributes to decrease the activation energy on the catalysts containing a small amount of phosphorous (vide infra).

3.6. Active sites on the catalysts

Recent studies on surface vanadium oxide species on oxide supports suggest that the bridging oxygen in the V–O–support bond is responsible for the catalytic activity for hydrocarbon oxidation [8,13,30]. Also in the selective oxidation of 3-picoline to nicotinic acid over V_2O_5/TiO_2 catalysts [6,7] the increase in the interface between vanadia and titania phases is the determining factor to improve the catalyst's activity. Monomeric vanadia species with vanadium tetrahedral coordination were formed, and the bridging oxygen in the V–O–Ti bond is suggested to be responsible for the catalytic activity. In the present work, based on the results of XRD and FT-IR, the change in crystal structure from $CrVO_4$-I to $CrVO_4$-III began to appear on $CrV_{1-x}P_xO_4$ when x exceeded 0.1 (Figs. 2 and 4). This structural change was accompanied by the decrease in the activity for the selective oxidation of 3-picoline to nicotinic acid (Fig. 5). Moreover, the amorphous phase was not active at all in this selective oxidation (Fig. 6). These results strongly suggest that the crystal structure, $CrVO_4$-I, in the $CrV_{1-x}P_xO_4$ catalysts played an important role on the catalytic activity.

We have briefly noted that the catalytic activity of $CrV_{1-x}P_xO_4$ may be due to the cooperation between the acid site and the reduction–oxidation property of VO_4 [18]. This was also suggested in the selective oxidation of 3-picoline over $Cr_{1-x}Al_xVO_4$ catalysts [14,15]. The structure of $CrVO_4$-I belongs to the α-$MnMoO_4$ type. In this vanadate, the Cr and V atoms replace the Mn and Mo, respectively, in order to form CrO_6 octahedra and VO_4 tetrahedra [21]. The arrangement of these polyhedra is totally different from the one in a stable $CrVO_4$-III form [orthorhombic *Cmcm*] [22]. In the latter structure, there are, along the (001) direction, chains of edge-sharing CrO_6 octahedra linked by VO_4 tetrahedra. On the other hand, the $CrVO_4$-I structure does not show any chain but does contain some clusters as in α-$MnMoO_4$. Indeed, it consists of an infinite network of Cr_4O_{16} clusters linked to the other clusters by VO_4 tetrahedra [21]. Nonetheless the VO_4 tetrahedra are separated well in both $CrVO_4$-I and $CrVO_4$-III, and the CrO_6 octahedra are more efficiently separated as the clusters in $CrVO_4$-I than as the chains in $CrVO_4$-III. Therefore, the V–O–Cr bond is more efficiently distributed in $CrVO_4$-I than in $CrVO_4$-III. This difference in the structure may affect the catalytic activity of the $CrVO_4$-I phase. The most potential candidate as the active sites is the isolated V sites bearing the reduction–oxidation properties assisted by Cr in the $CrVO_4$-I structure.

The replacement of V with a small amount of P in $CrVO_4$-I resulted in an increase in the activity (Fig. 5). Activation energies of the $CrV_{1-x}P_xO_4$ catalyst were calculated from the rate of 3-picoline consumption at 300–400 °C in the presence of water (molar ratio of water/3-picoline: 10.8) and are shown in Fig. 13. Evidently the lowest value was observed with $CrV_{0.95}P_{0.05}O_4$(570), which coincided well with the order of the activity of $CrV_{1-x}P_xO_4$ catalysts. Upon increasing the amount of P incorporated in the catalyst, the activation energy was substantially changed, suggesting that the nature of the active site gradually changed with increasing amounts of P. The replacement of V with

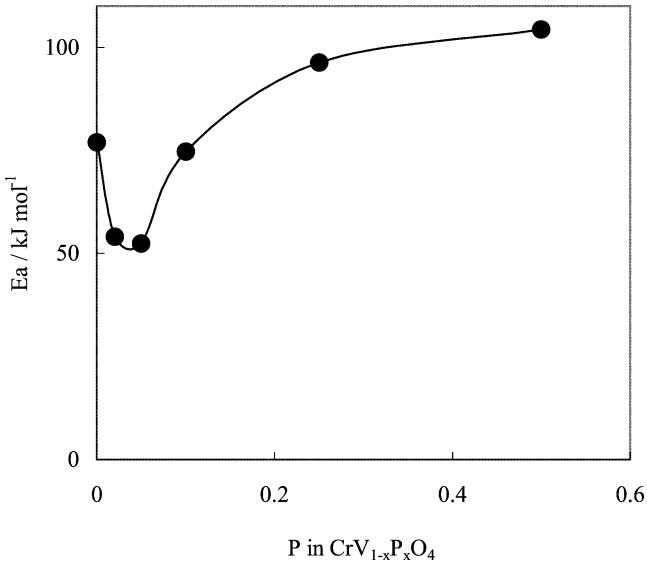

Fig. 13. Apparent activation energy of the oxidation of 3-picoline over $CrV_{1-x}P_xO_4$.

a small amount of P was effective for lowering the activation energy, suggesting that the nature of the reduction–oxidation sites is substantially affected by the presence of P. It is thus concluded that the reduction–oxidation property of V assisted by a small amount of P reveals a definitive role in the rate-determining step of 3-picoline oxidation. Moreover, the V(–P) reduction–oxidation sites are assisted by the efficiently distributed V–O–Cr bonds in the $CrVO_4$-I type crystal structure. The rate-determining step may be a H-abstraction from 3-picoline or an oxygen insertion into an active intermediate formed from 3-picoline.

On the other hand, Brönsted acid sites may be effective for the activation of 3-picoline and/or the desorption of nicotinic acid formed on the catalyst surface. The amount of this acid site was enormously enhanced by the addition of water, and this fact was apparently explained by the conversion of Lewis acid sites to Brönsted acid sites. The role of water should also be given in the hydrolysis of V–O–P bonds resulting in the erection of new Brönsted acid sites. The higher acidity may result particularly in the enhancement of selectivity, probably due to better desorption of the formed acid, which will be protected from further total oxidation. The acid sites are thus important for assisting the selective oxidation of 3-picoline to nicotinic acid on the V sites, while the V sites reveal key role in the selective oxidation 3-picoline by their reduction–oxidation cycles assisted by Cr as well as by a small amount of P.

4. Conclusion

$CrV_{1-x}P_xO_4$ catalysts were prepared as the crystalline form from the aqueous solution of raw materials and tested for the selective oxidation of 3-picoline to nicotinic acid. $CrV_{1-x}P_xO_4$ ($x \leqslant 0.1$) has mainly a monoclinic $CrVO_4$-I crystal structure belonging to the α-$MnMoO_4$ type, while the orthorhombic $CrVO_4$-III structure appeared when the value of x exceeded 0.25. There are chains of edge-sharing CrO_6 octahedra linked by VO_4 tetrahedra in $CrVO_4$-III, while the $CrVO_4$-I structure does not show any chain but consists of an infinite network of Cr_4O_{16} clusters linked to the other clusters by VO_4 tetrahedra. Therefore, the V–O–Cr bond is more efficiently distributed in $CrVO_4$-I than in $CrVO_4$-III and may affect the catalytic activity of the $CrVO_4$-I phase. The activity changed depending on the P content, and $CrV_{0.95}P_{0.05}O_4$ showed the highest activity for the selective oxidation as well as the lowest activation energy of the 3-picoline conversion, and the activity decreased with increasing P content. A partial replacement of V with P resulted in a significant increase in the activity probably due to modification of the reduction–oxidation properties of V–O–Cr sites. Water addition enormously enhanced the selective oxidation of 3-picoline to nicotinic acid by erecting Brönsted acid sites on the catalyst surface. At 360 °C, 3-picoline was selectively oxidized to nicotinic acid and pyridine-3-carbaldehyde with a total yield of 84% at a conversion of 93%. It is concluded that the active sites on the $CrV_{0.95}P_{0.05}O_4$ catalyst for the selective oxidation are the V reduction–oxidation sites assisted by both Cr and P as well as by the Brönsted acidic properties.

References

[1] W.F. Hoelderich, Appl. Catal. A 194–195 (2000) 487.
[2] A. Martin, B. Lucke, Catal. Today 57 (2000) 61.
[3] A. Andersson, J. Catal. 100 (1986) 414.
[4] S. Järås, S.T. Lundin, J. Appl. Chem. Biotechnol. 27 (1977) 499.
[5] S. Lars, T. Andersson, S. Järås, J. Catal. 64 (1980) 51.
[6] D. Heinz, W.F. Hoelderich, S. Krill, W. Boech, K. Huthmacher, J. Catal. 192 (2000) 1.
[7] E.M. Al'kaeva, T.V. Andrushkevich, G.A. Zenkovets, G.N. Kryukova, S.V. Tsybulya, E.B. Burgina, Catal. Today 61 (2000) 249.
[8] E.M. Al'kaeva, T.V. Andrushkevich, G.A. Zenkovets, D.E. Babushkin, Catal. Lett. 54 (1998) 149.
[9] A. Andersson, J. Catal. 76 (1982) 144.
[10] A. Martin, B. Lucke, H.-J. Niclas, A.A. Forster, React. Kinet. Catal. Lett. 43 (1991) 583.
[11] M. Gasior, J. Haber, T. Machej, Appl. Catal. 33 (1987) 1.
[12] J. Zhu, L.T. Andersson, Appl. Catal. 53 (1989) 251.
[13] D.A. Bulushev, L. Kiwi-Minsker, V.I. Zaikovskii, A. Renken, J. Catal. 193 (2000) 145.
[14] Z. Song, E. Kadowaki, T. Shishido, Y. Wang, K. Takehira, Chem. Lett. (2001) 754.
[15] Z. Song, E. Kadowaki, T. Shishido, Y. Wang, K. Takehira, Appl. Catal. A 239 (2003) 287.
[16] J.P. Attfield, J. Solid State Chem. 67 (1987) 58.
[17] R.D. Shannon, Acta Crystallogr. A 32 (1976) 751.
[18] Z. Song, T. Matsushita, T. Shishido, T. Takehira, Chem. Commun. (2002) 1306.
[19] E. Baudrin, S. Denis, F. Orsini, L. Seguin, M. Touboul, J.-M. Tarascon, J. Mater. Chem. 9 (1999) 101.
[20] M. Touboul, K. Melghit, J. Mater. Chem. 5 (1995) 147.

[21] M. Touboul, S. Denis, D. Seguin, Eur. J. Solid State Inorg. Chem. 32 (1995) 577.
[22] M.J. Isasi, R. Saez-Puche, M.L. Veiga, C. Pico, A. Jerez, Mater. Res. Bull. 23 (1988) 595.
[23] E.J. Baran, J. Mater. Sci. 33 (1998) 2479.
[24] M. Touboul, K. Melghit, P. Benard, Eur. J. Solid State Inorg. Chem. 31 (1994) 151.
[25] M. Touboul, P. Toledano, Acta Crystallogr. B 36 (1980) 240.
[26] S.J. Puttock, C.H. Rochester, J. Chem. Soc., Faraday Trans. 1 82 (1986) 2773.
[27] L. Savary, J. Saussey, G. Costentin, M.M. Bettahar, M. Gubelmann-Bonneau, J.C. Lavalley, Catal. Today 32 (1996) 57.
[28] G. Busca, Catal. Today 41 (1998) 191.
[29] H.W. Zanthoff, M. Sananes-Schultz, S.A. Buchholz, U. Rodemerck, B. Kubias, M. Baerns, Appl. Catal. A 172 (1998) 49.
[30] I.E. Wachs, B.M. Weckhuysen, Appl. Catal. A 157 (1997) 67.